Inorganic Chemistry
Article

Inorg. Chem. **2011**, *50*, 827–835 **827**
DOI: 10.1021/ic101720m

Planar Symmetry Incompatibility in Ru−Sn−Zn Pseudo-Decagonal Approximants Composed of Novel Pentagonal Antiprisms

Ding-Bang Xiong,*,†,‡ Norihiko L. Okamoto,‡ and Haruyuki Inui‡

†*Department of Chemistry and Center of Material Sciences, Philipps University Marburg, Hans-Meerwein-Strasse, 35032 Marburg, Germany, and* ‡*Department of Materials Science and Engineering, Kyoto University, Kyoto 606-8501, Japan*

Received June 20, 2010

Two new ternary compounds in the Ru−Sn−Zn system were synthesized by conventional high-temperature reactions, and their crystal structures were analyzed by means of the single crystal X-ray diffraction: $Ru_2Sn_2Zn_3$ (orthorhombic, *Pnma*, Pearson symbol *oP*28, $a = 8.2219(16)$, $b = 4.1925(8)$, $c = 13.625(3)$ Å, $V = 469.66(16)$ Å^3, $Z = 4$) and $Ru_{4.15}Sn_{4.96}Zn_{5.85}$ (orthorhombic, *Pnma*, Pearson symbol *oP*60-δ, $a = 8.3394(17)$, $b = 4.2914(9)$, $c = 28.864(6)$ Å, $V = 1032.98(40)$ Å^3, $Z = 4$). With the increase in the Sn content, the half-decagon structure unit with a triangle center in $Ru_2Sn_2Zn_3$ grows up to a symmetry incompatible decagonal unit with a central triangle in the common plane in $Ru_{4.15}Sn_{4.96}Zn_{5.85}$. Both structures can be described by hexagonal arrays of Sn-centered novel pentagonal antiprisms. In light of their pseudodecagonal diffraction in the *h*0*l* section and point group *mmm*, both phases are considered as new quasicrystal approximants in the Ru−Zn−Sn ternary system. The temperature dependences of the electrical resistivity for both compounds exhibit metallic behavior, but their Seebeck coefficients are of opposite sign.

Introduction

Usually, it is expected that the symmetries of two concentric coordinated polyhedrons or coaxial polygons in local atomic configuration will be the same or in a group−subgroup relationship; otherwise, it is considered as symmetry incompatibility. Symmetry incompatibility usually results in disordered or distorted structure units as reported in both periodic and quasiperiodic structures.[1−3] For example, because the 5-fold axis is incompatible with crystallographic symmetries, disorders are very common in the structures with icosahedral units. In stable binary MCd_6 (M = Ca, rare-earth) icosahedral quasicrystals and crystalline approximants,[1] the symmetry incompatibility between the clusters with icosahedral (I_h) and tetrahedral symmetry (T_d) resulted in the significantly disordered Cd_4 tetrahedra. The structures with disorders caused by symmetry incompatibility were also observed in other examples, such as the complex intermetallic phase ruthenium zinc antimonides[2] and gallium cluster in organometallic compound.[3] In addition to disorder, the distortion of an icosahedral shape leading to the loss of the 5-fold rotational symmetry is the other example. Interestingly, however, although two types of symmetry cannot be expressed through group−subgroup relationships, they can coexist in many structures if one is latent in the other.[4] Alvarez and his co-workers, by geometric analysis of a variety of molecular and crystal structures, revealed that partial augmentation of the elements (faces, edges, or vertices) of a icosahedral (I_h) polyhedron can produce an octahedral symmetry (O_h).[4] These two incompatible symmetries can be combined in a cubic structure without disorder or distortion as indicated by *continuous symmetry and shape measurements* (*CSM* and *CShM*).[4,5]

Symmetry incompatibilities in all the compounds mentioned above are three-dimensional cases, which combine the icosahedral symmetry (I_h) with a certain crystallographic one, but two-dimensional (planar) cases are rare. In this work, we report the growth of a planar symmetrically incompatible structural unit in the Ru−Sn−Zn system, a decagon with a central triangle in a common plane. With the increase in the Sn content from phase $Ru_2Sn_2Zn_3$ to $Ru_{4.15}Sn_{4.96}Zn_{5.85}$, the half decagonal unit grows up to a full decagonal one, while the central triangles are present in both phases. Because of the resemblance between the triangle-centered full decagon and Gummelt decagon,[6] the formation ability of quasicrystals

*To whom correspondence should be addressed. E-mail: xiong.dingbang@ky8.ecs.kyoto-u.ac.jp.

(1) (a) Tsai, A. P.; Guo, J. Q.; Abe, E.; Takakura, H.; Sato, T. J. *Nature* **2000**, *48*, 537–538. (b) Guo, J. Q.; Abe, E.; Tsai, A. P. *Phys. Rev. B* **2000**, *62*, 14605–14608. (c) Pay Gómez, C.; Lidin, S. *Phys. Rev. B* **2003**, *68*, 024203.

(2) Xiong, D. B.; Zhao, Y. F.; Schnelle, W.; Okamoto, N. L.; Inui, H. *Inorg. Chem.* **2010**, *49*, 10788–10797.

(3) Kehrwald, M.; Köstler, W.; Rodig, A.; Linti, G.; Blank, T.; Wiberg, N. *Organometallics* **2001**, *20*, 860–867.

(4) Echeverría, J.; Casanova, D.; Llunell, M.; Alemany, P.; Alvarez, S. *Chem. Commun.* **2008**, 2717–2725.

(5) (a) Zabrodsky, H.; Peleg, S.; Avnir, D. *J. Am. Chem. Soc.* **1992**, *114*, 7843–7851. (b) Alvarez, S.; Alemany, P.; Casanova, D.; Cirera, J.; Llunell, M.; Avnir, D. *Coord. Chem. Rev.* **2005**, *249*, 1693–1708.

Published on Web 01/06/2011

Table 1. Nominal Compositions, Products, Estimated Yields, and EDS Results in Different Reactions

reaction	nominal composition	main phases (composition from EDS)
I	$Ru_4Sn_4Zn_6$	~90% $Ru_2Sn_2Zn_3$ ($Ru_{27.4}Sn_{29.0}Zn_{43.6}$) ~10% $Ru_{4.15}Sn_{4.96}Zn_{5.85}$ ($Ru_{26.2}Sn_{33.9}Zn_{39.9}$)
II	$Ru_4Sn_5Zn_6$	~90% $Ru_{4.15}Sn_{4.96}Zn_{5.85}$ ($Ru_{25.9}Sn_{33.4}Zn_{40.7}$) ~10% $Ru_2Sn_2Zn_3$ ($Ru_{27.6}Sn_{29.3}Zn_{43.1}$)
III	$Ru_4Sn_4Zn_4$	~50% $Ru_2Sn_2Zn_3$, ~50% unidentified phases
IV	$Ru_4Sn_xZn_{11}$ (x = 2.1, 2.9, 3.3, 3.6)	85−98% $Ru_4Sn_{2.9}Zn_{11.6}$ ($Ru_{21.4}Sn_{15.5}Zn_{63.1}$)[7]
V	$Ru_4Sn_{1.6}Zn_{30.4}$	$RuZn_{7.6}Sn_{0.4}$[8]

Table 2. Crystallographic and Technical Data of the Single Crystal Structure Refinements of $Ru_2Sn_2Zn_3$ and $Ru_{4.15}Sn_{4.96}Zn_{5.85}$

chemical formula	$Ru_2Sn_2Zn_3$	$Ru_{4.15}Sn_{4.96}Zn_{5.85}$
EDS	$Ru_{1.9(7)}Sn_{2.0(8)}Zn_{3.1(5)}$	$Ru_{3.9(7)}Sn_{4.8(9)}Zn_{6.1(5)}$
M_r	635.63	1391.21
space group, Z	*Pnma* (No. 62), 4	
Pearson symbol	*oP*28	*oP*60−δ
a, Å	8.2219(16)	8.3394(17)
b, Å	4.1925(8)	4.2914(9)
c, Å	13.625(3)	28.864(6)
V, Å^3	469.66(16)	1032.98(40)
D_c, g cm^{-3}	8.989	8.946
μ, mm^{-1}	32.44	30.86
crystal size, mm^3	0.24 × 0.18 × 0.16	0.17 × 0.16 × 0.10
θ_{max}, deg	29.89	33.01
reflns collected, R_{int}	3785/0.0579	12656/0.0811
index range, *hkl*	−11 to 10, −5 to 5, −18 to 19	−12 to 12, −6 to 6, −40 to 44
min/max transmission	0.0266/0.0638	0.0218/0.0751
data/variables	732/44	2169/91
obs. reflections ($I_o > 2\sigma(I_o)$)	703	1669
$R(F)^a$ ($I_o > 2\sigma(I_o)$)	0.0369	0.0450
$R(F)$ (all data)	0.0386	0.0594
$wR(F^2)^b$ (all data)	0.0916	0.1084
goodness of fit (F^2)	1.193	1.053
$\Delta\rho_{min}/\Delta\rho_{max}$, e Å^3	−2.362/2.327	−3.503/2.825

[a] $R = \sum||F_o| - |F_c||/\sum|F_o|$. [b] $wR = \{\sum[w(F_o^2 - F_c^2)^2]/\sum[w(F_o^2)^2]\}^{1/2}$.

and approximants in this system was also discussed. Another unique feature of these two structures is the presence of a novel pentagonal antiprism which is different from an interpenetrating icosahedral antiprism. The transport properties of both compounds were characterized.

Experimental Section

Synthesis and Phase Analysis. All samples (**I**−**V** in Table 1) were prepared via high-temperature reaction of ruthenium (3 N), zinc (4 N), and tin (3 N) in evacuated fused-silica ampules. The ampules were heated at the rate of 60 K/h up to 1273 K and maintained at this temperature for 5 h, followed by a temperature decrease to 923 K at the rate of 50 K/h. The ampules were held at 923 K for 4 days and then slowly cooled down to room temperature in a furnace. The purities of the as-produced samples were checked by powder X-ray diffraction (XRD). Rough Rietveld refinements (Supporting Information Figure S1) indicated that the phases $Ru_2Sn_2Zn_3$ and $Ru_{4.15}Sn_{4.96}Zn_{5.85}$ coexisted in the products of the reactions **I** and **II**, and the estimated weight percentage of the main phase in each reaction was close to 90%. Energy dispersion spectroscopy (EDS) results showed that the crystals from different reactions for each phase had almost the same composition, which indicated that the solubility regions of these two phases were narrow. The nominal compositions, products, and EDS results for the five different reactions are listed in Table 1.

Crystal Structure Determination. Single-crystal XRD intensities were recorded with an imaging plate diffractometer (IPDS, Stoe & Cie.) operated with Mo Kα radiation (λ = 0.71069 Å) at room temperature. At least three crystals for each phase from the samples with different purities were studied by the single-crystal XRD method. A numerical absorption correction based

Table 3. Atomic Coordinates (Å), Equivalent Displacement Parameters (Å^2), and Occupation Factors of $Ru_2Sn_2Zn_3$ and $Ru_{4.15}Sn_{4.96}Zn_{5.85}$

atom[a]	x	y	z	U_{eq}[b], U_{iso}*	occ.
			$Ru_2Sn_2Zn_3$		
Sn1	0.15309(6)	1/4	0.69623(4)	0.0082(2)	1.0
Sn2	0.65020(6)	1/4	0.47543(4)	0.0077(2)	1.0
Ru1	0.45766(8)	1/4	0.64112(4)	0.0075(2)	1.0
Ru2	0.84783(7)	1/4	0.63111(5)	0.0065(2)	1.0
Zn1	0.03450(14)	1/4	0.45847(8)	0.0151(3)	1.0
Zn2	0.34237(11)	1/4	0.37046(8)	0.0102(3)	1.0
Zn3	0.58993(11)	1/4	0.24434(6)	0.0103(3)	1.0
			$Ru_{4.15}Sn_{4.96}Zn_{5.85}$		
Sn1	0.00474(8)	1/4	0.72557(3)	0.01510(16)	1.0
Sn2	0.51668(8)	1/4	0.62392(3)	0.01630(15)	1.0
Sn3	0.30198(8)	1/4	0.45347(3)	0.01525(15)	1.0
Sn4	0.69696(8)	1/4	0.46041(3)	0.01693(16)	1.0
Sn5	0.82935(9)	1/4	0.34463(3)	0.0182(3)	0.963(5)
Ru1	0.31235(9)	1/4	0.69626(3)	0.01395(17)	1.0
Ru2	0.70008(9)	1/4	0.69774(3)	0.01318(17)	1.0
Ru3	0.49789(9)	1/4	0.53479(3)	0.01315(16)	1.0
Ru4	0.99397(9)	1/4	0.42460(3)	0.01313(17)	1.0
Zn1	0.18199(16)	1/4	0.34496(5)	0.0190(3)	1.0
Zn2	0.49048(14)	1/4	0.30684(5)	0.0161(2)	1.0
Zn3	0.23515(15)	1/4	0.25207(4)	0.0174(2)	1.0
Zn4	0.98556(18)	1/4	0.52208(5)	0.0215(3)	1.0
Zn5	0.87448(19)	1/4	0.61323(5)	0.0250(3)	1.0
Zn61	0.1977(2)	1/4	0.59221(7)	0.025*[c]	0.84
Ru62	0.1787(9)	1/4	0.6050(3)	0.025*[c]	0.16

[a] All atoms are in Wyckoff sites of 4*c*. [b] U_{eq} is defined as one-third of the trace of the orthogonalized U_{ij} tensor. [c] Fixed U_{iso}.

(6) (a) Gummelt, P. *Geometriae Dedicata* **1996**, *62*, 1–17. (b) Gummelt, P. *Mater. Sci. Eng., A* **2000**, *294*, 250–253.

Table 4. Selected Interatomic Distances (Å) in the Structure of $Ru_2Sn_2Zn_3$ and $Ru_{4.15}Sn_{4.96}Zn_{5.85}$

$Ru_2Sn_2Zn_3$

Sn1—	Ru1	2.614(1)	Ru2—	Zn1 × 2	2.612(1)	Zn2—	Zn3	2.599(1)
	Ru2	2.662(1)		Zn2 × 2	2.615(1)		Ru2 × 2	2.615(1)
	Ru1	2.737(1)		Zn3 × 2	2.653(1)		Zn3	2.664(1)
	Ru2	2.846(1)		Sn1	2.662(1)		Ru1 × 2	2.669(1)
	Zn3 × 2	2.969(1)		Sn2	2.672(1)		Zn1	2.801(2)
	Zn3 × 2	3.084(1)		Zn1	2.809(1)		Sn2	2.907(1)
	Zn2 × 2	3.167(1)		Sn1	2.846(1)		Sn2 × 2	2.968(1)
				Ru1	3.211(1)		Sn1 × 2	3.167(1)
Sn2—	Ru2	2.672(1)		Ru1	3.232(1)			
	Ru1	2.757(1)				Zn3—	Zn2	2.599(1)
	Ru1 × 2	2.775(1)	Zn1—	Zn1 × 2	2.449(1)		Ru1 × 2	2.643(1)
	Zn2	2.907(1)		Ru2 × 2	2.612(1)		Ru2 × 2	2.653(1)
	Zn2 × 2	2.968(1)		Zn3	2.801(1)		Zn2	2.664(1)
	Zn1	3.168(1)		Zn2	2.801(2)		Zn1	2.801(1)
	Zn3	3.187(1)		Ru2	2.809(1)		Sn1 × 2	2.969(1)
				Sn2	3.168(1)		Sn1 × 2	3.084(1)
Ru1—	Zn3 × 2	2.643(1)					Sn2	3.187(1)
	Zn2 × 2	2.669(1)						
	Sn1	2.737(1)						
	Sn1	2.614(1)						
	Sn2	2.757(1)						
	Sn2 × 2	2.775(1)						
	Ru2	3.211(1)						
	Ru2	3.232(1)						

$Ru_{4.15}Sn_{4.96}Zn_{5.85}$

Sn1—	Ru2	2.665(1)	Ru1—	Zn2 × 2	2.705(1)	Zn2—	Zn3	2.652(2)
	Ru1	2.701(1)		Ru1	2.695(1)		Zn3	2.656(2)
	Ru2	2.749(1)		Zn3 × 2	2.712(1)		Ru2 × 2	2.673(1)
	Ru1	2.769(1)		Sn5 × 2	2.719(1)		Ru1 × 2	2.705(1)
	Zn3 × 2	3.004(1)		Sn1	2.701(1)		Zn1	2.798(2)
	Zn3 × 2	3.146(1)		Sn1	2.769(1)		Sn2 × 2	2.933(1)
	Zn2 × 2	3.179(1)		Ru62	2.859(7)		Sn5	3.029(2)
	Sn5 × 2	3.260(1)		Zn61	3.152(2)		Sn1 × 2	3.180(1)
				Ru2	3.200(2)			
Sn2—	Ru3	2.577(1)		Ru2	3.234(2)	Zn3—	Ru2 × 2	2.645(1)
	Ru2	2.623(1)					Zn2 × 2	2.656(2)
	Ru1	2.695(1)	Ru2—	Zn3 × 2	2.645(1)		Ru1 × 2	2.712(1)
	Zn61	2.813(2)		Ru2	2.623(1)		Zn1	2.717(2)
	Ru62	2.870(7)		Zn1 × 2	2.663(1)		Sn5	2.900(2)
	Zn2 × 2	2.933(1)		Sn1	2.665(1)		Sn1 × 2	3.004(1)
	Zn5	3.000(2)		Zn2 × 2	2.673(1)		Sn1 × 2	3.146(1)
				Sn1	2.748(1)			
Sn3—	Ru4	2.701(1)		Zn5	2.840(2)	Zn4—	Zn4 × 2	2.507(1)
	Ru3 × 2	2.740(1)		Ru1	3.200(2)		Ru4 × 2	2.646(1)
	Ru3	2.860(1)		Ru1	3.234(2)		Zn61	2.688(3)
	Sn4 × 2	3.284(1)					Zn5	2.789(2)
	Zn5 × 2	3.237(1)	Ru3—	Sn4 × 2	2.695(1)		Ru4	2.814(1)
	Zn1	3.288(1)		Ru3	2.577(1)		Ru62	2.886(7)
	Zn4 × 2	3.294(1)		Sn4	2.714(1)		Sn4	2.994(2)
	Zn4	3.299(1)		Sn3 × 2	2.739(1)		Sn3 × 2	3.294(1)
	Sn4	3.300(1)		Sn3	2.860(1)		Sn3	3.299(1)
				Ru3 × 2	2.939(1)			
Sn4—	Ru4	2.684(1)		Zn61	3.002(2)	Zn5—	Zn1 × 2	2.506(1)
	Ru3 × 2	2.695(1)					Ru62	2.581(6)
	Ru3	2.714(1)	Ru4—	Zn5 × 2	2.646(1)		Ru4 × 2	2.646(1)
	Zn61 × 2	2.772(1)		Zn4 × 2	2.646(1)		Zn61	2.763(3)
	Ru62 × 2	3.041(5)		Sn4	2.684(1)		Zn4	2.790(2)
	Zn4	2.994(2)		Sn5	2.686(1)		Ru2	2.840(2)
	Sn3 × 2	3.284(1)		Sn3	2.701(1)		Sn2	3.001(2)
	Sn3	3.300(2)		Zn61 × 2	2.719(1)		Sn3 × 2	3.237(1)
				Ru62 × 2	2.722(5)			
Sn5—	Ru62 × 2	2.592(4)		Zn1	2.783(2)	Zn61—	Zn4	2.688(3)
	Ru4	2.686(1)		Zn4	2.814(2)		Ru4 × 2	2.719(1)
	Ru1 × 2	2.719(1)					Sn4 × 2	2.772(1)
	Zn61 × 2	2.825(2)	Zn1—	Zn5 × 2	2.506(1)		Zn5	2.763(3)
	Zn3	2.900(2)		Ru2 × 2	2.663(1)		Sn5 × 2	2.825(2)
	Zn1	2.941(2)		Zn3	2.718(2)		Sn2	2.813(2)
	Zn2	3.029(2)		Ru4	2.783(2)		Ru3	3.002(2)
	Sn1 × 2	3.260(1)		Zn2	2.798(2)		Ru1	3.152(2)
				Sn5	2.941(2)			
				Sn3	3.288(1)	Ru62—	Zn5	2.548(7)
							Sn5 × 2	2.592(4)
							Ru4 × 2	2.722(5)
							Ru62	2.581(6)
							Zn4	2.886(7)
							Sn2	2.870(7)
							Ru1	2.859(7)
							Sn4 × 2	3.041(5)

on the sizes and shapes of the crystals was applied to the data sets. Then the structures were solved by applying the direct method, and all atoms were given directly. Subsequently the structures were refined on F^2 with a full-matrix least-squares algorithm using the program *SHELXTL*, version 6.1.[9] Both structures crystallize in the orthorhombic system with the space group of *Pnma*. The structures were finally refined with anisotropic displacement parameters. In the refinement, the site occupancy factors (SOFs) were checked for deviation from unity by freeing SOF of an individual atom while the remaining SOFs were fixed. The sites with SOF deviating from unity by less than twice the standard deviation were considered as being fully occupied. All seven crystallographically distinct sites were fully occupied in $Ru_2Sn_2Zn_3$ (Table 3).

In the refinement of $Ru_{4.15}Sn_{4.96}Zn_{5.85}$, however, the Sn5 and Zn6 sites were exceptions. The SOF of the Sn5 site deviated from unity by about eight times the standard deviation, and it was considered to be partially occupied with the refined fraction of 0.96. Checked in the same way, the Zn6 site was also confirmed to be partially occupied. However, there existed another obvious residual peak (the intensities of the first two strongest residual peaks were 4.33 and 2.40 e/Å^3) having short distances (0.7 Å) to Zn6, no matter the Zn6 was refined as the partially or fully occupied one. And then the Zn6 site together with the strongest residual peak were refined as a split site and assigned as Zn61 and Zn62, respectively. Compared with the closely related $Ru_2Sn_2Zn_3$ in this work, however, the bond length of Zn62−Sn5 (2.620(3) Å) was too short because the shortest Zn−Sn bond length was more than 2.90 Å in $Ru_2Sn_2Zn_3$. Carefully checking other contacts, the bond length appears to be more reasonable if the Zn62 was assigned as a Ru atom (namely, Ru62 in Table 3). The isotropic displacement parameters U_{iso} for Ru62 (0.0303(16) Å^2) seems anomalously larger than that for other Ru atoms with the average of 0.0135 Å^2 in the structure, which might be correlated with the occupancy on this site. And then the U_{iso} value for Ru62 was constrained to be equal to that of its partner Zn61 in the split position, approximately 0.25. Finally, the Zn6 site was refined as split between Zn61 and Ru62, constrained to have a total occupation of 1.0.

ADDSYM routine in *PLATON*[10] reported the existence of a missed symmetry *I* (body-centered) in the structure of $Ru_{4.15}Sn_{4.96}Zn_{5.85}$. Subsequently, we checked the statistic on the system absence and found that there were 2570 (with $I_0 > 3\sigma(I_0)$) of the total 6595 reflections disobeying the exception for the *I* lattice. The averaged intensity of these 2570 reflections was about one-fifth of that for the disobeying reflections if the structure was assumed as a base-centered (*A*, *B*, and *C*) or face-centered (*F*) orthorhombic lattice. And then the structure was refined with the space group of *Imma*, which converged with $R_1 = 4.37\%$ for all data, and the obtained formula $Ru_6Sn_4Zn_5$ was far from the EDS results. Although we can obtain the $Ru_4Sn_5Zn_6$ by modeling one of the Ru sites as mixed between Sn and Zn, the space group *Pnma* was supported by comparing the experimental powder XRD pattern with the simulated patterns using structural models with two different space groups (Supporting Information Figure S3). We turned back to the structural model with the space group *Pnma*, checked the atomic coordinates carefully, and found that nearly all atoms in the *ac* plane were related by pseudo mirror planes perpendicular to the *a* axis at $x = 0.0$ and 0.5 ((Δx;Δz): the numbers in brackets correspond to the displacements necessary to obtain a structure having the mirror planes as real symmetry elements): Sn1 (0.005;0.0), Sn2 (0.017;0.0), Ru3 (0.002;0.0), Ru4 (0.006;0.0), Zn2 (0.01;0.0), Zn3 (0.0;0.004), and Zn4 (0.014;0.0) replicated themselves, and Sn3−Sn4 (0.001;0.007), Sn5−Zn1 (0.01;0.0), Ru1−Ru2 (0.012;0.001), and Zn5−Zn61(Ru62) (0.07(0.06);0.02(0.01)) were related atom pairs. Apart from the Zn5, splitting Zn6, and heteroatom pair Sn5−Zn1, the combination of these atoms and atom pairs fulfills well the symmetry requirements of mirror planes, allowing for minor imperfections. If so, a structure model with the space group of *Imma* ($I\,2_1/m\,2_1/m\,2_1/a$) will be realized by appropriately shifting the origin of the unit cell with the space group of *Pnma* (Supporting Information Figure S4). Therefore, the detected missed symmetry *I* should be a pseudo symmetry. Finally, the structure was refined with the space group of *Pnma*, and least-squares refinements with anisotropic parameters converged at $R1 = 4.50\%$, $wR2 = 10.82\%$, GOF = 1.084 for 91 parameters, and 1669 independent reflections ($I > 2\sigma(I)$). The refined formula $Ru_{4.15}Sn_{4.96}Zn_{5.85}$ is in excellent agreement with the EDS results.

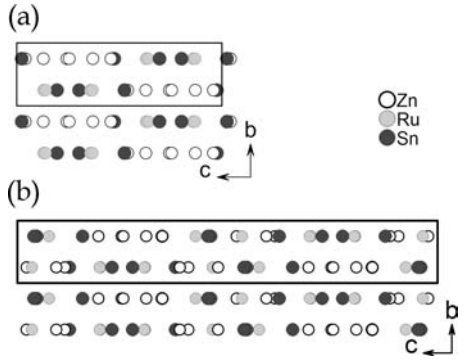

Figure 1. Projections of the structures of $Ru_2Sn_2Zn_3$ (a) and $Ru_{4.15}Sn_{4.96}Zn_{5.85}$ (b) along the *a* axis. The rectangles indicate the unit cells.

Additional details concerning data collection and crystallographic data are summarized in Table 2. Tables 3 and 4 list the positional and occupational parameters together with the equivalent displacement parameters U_{eq} and selected interatomic distances. Further details of the crystal structure investigations can be obtained from the Fachinformationszentrum Karlsruhe, D-76344 Eggenstein-Leopoldshafen, Germany (fax: (+49) 7247-808-666; e-mail: crysdata@fiz.karlsruhe.de) on quoting the depository numbers CSD-421663 and CSD-421664 for $Ru_2Sn_2Zn_3$ and $Ru_{4.15}Sn_{4.96}Zn_{5.85}$, respectively.

Transport Property Measurement. For the measurement of thermoelectric properties in the middle temperature range from 323 to 660 K, fine grain and homogeneous powder was hot-pressed in a high-density graphite die at 873 K for approximately 30 min under the pressure of 50 MPa. The densities for both samples are about 75% of the theoretical value. Rectangular specimens with the dimensions of $\sim 2.5 \times 2 \times 7$ mm^3 were cut from the hot-pressed samples by electric discharge machining for measurements of the Seebeck coefficient and electrical resistivity. Measurements of the Seebeck coefficient and electrical resistivity were made with an ULVAC ZEM-2 apparatus, with measurement errors of less than ±10%. Values of thermal conductivity were estimated from those of thermal diffusivity and specific heat measured by the laser flash method with a ULVAC TC-7000 apparatus for thin-disk specimens with a diameter of 10 mm and a thickness of ~1.2 mm. The value of heat capacity C_p at room temperature is the only one available in our experiments.

Results and Discussion

Structural Features. Both $Ru_2Sn_2Zn_3$ and $Ru_{4.15}Sn_{4.96}Zn_{5.85}$ exhibit new structure types and crystallize in the space group of *Pnma* (Figure 1). The structures can be decomposed into absolutely flat atomic layers parallel to the

(7) Xiong, D. B.; Yang, K.; Zhao, Y. F.; Ma, J. *Dalton Trans.* **2010**, *39*, 8331–8338.
(8) Kuntze, R.; Hillebrecht, H. *Z. Kristallogr. Suppl.* **2007**, *21*, 079–50.
(9) *SHELXTL*; Bruker AXS, Inc.: Madison, WI, 2000.
(10) (a) Le Page, Y. *J. Appl. Crystallogr.* **1987**, *20*, 264–269. (b) Spek, A. L. *J. Appl. Crystallogr.* **2003**, *36*, 7–13.

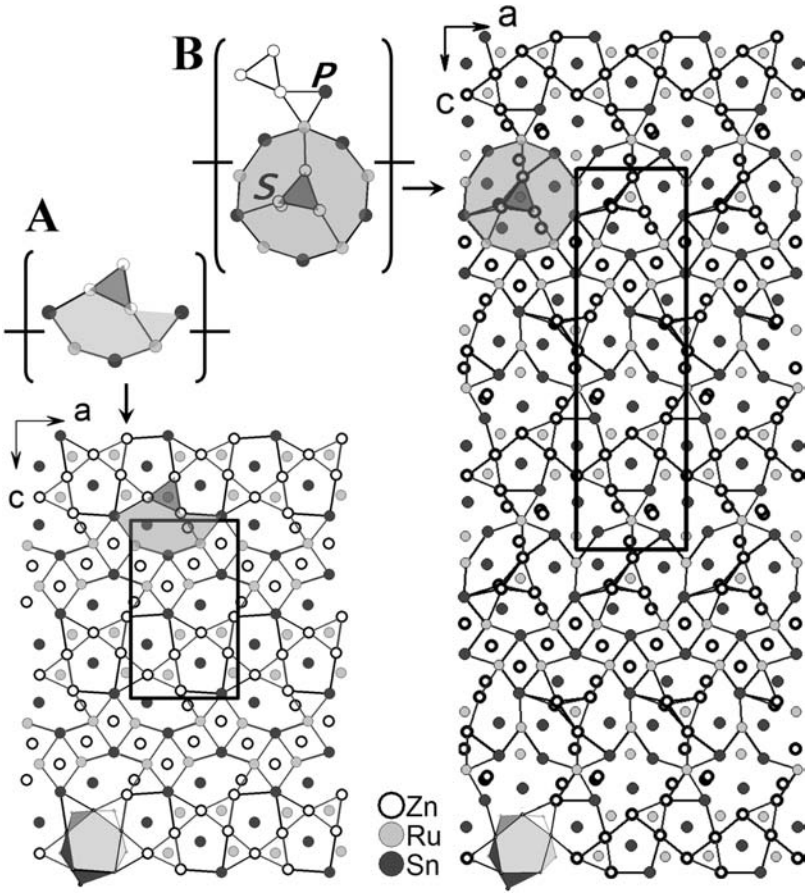

Figure 2. Layers parallel to the (010) plane in the structures of $Ru_2Sn_2Zn_3$ (left) and $Ru_{4.15}Sn_{4.96}Zn_{5.85}$ (right). The structural unit **A** consisting of a half decagon and a Zn_3 triangle in $Ru_2Sn_2Zn_3$ grows up to the structural unit **B** consisting of a full decagon, a central $Zn_{2.84}Ru_{0.16}$ triangle, and branches in $Ru_{4.15}Sn_{4.96}Zn_{5.85}$. The atomic site marked with **P** is slightly deficient while that marked with **S** splits into two sites. The layers at the height of $y = 0.75$ is indicated by nets, and the atoms without linking are located in the layers at the height of $y = 0.25$. Pentagonal antiprisms (will be discussed later) are highlighted at the bottom left in each crystal structure. The rectangles indicate the unit cells.

(010) plane (Figure 2). One has to keep in mind, however, that the chemical bonding within and between the layers is of the same character. There are no preferred cleavage planes. In $Ru_2Sn_2Zn_3$, the structure building unit (SBU) in the layer is a half decagon Ru_2Sn_3 with Zn_3 triangle, namely, unit **A** in Figure 2. SBUs **A** connect to one another along the *a* axis to form a linear row. The neighboring rows are parallel to each other, and they are with opposite orientations. The centers of Zn3 triangles in two neighboring rows shift along the *a* axis by the radius of the half decagon. In $Ru_{4.15}Sn_{4.96}Zn_{5.85}$, the half decagon in SBU **A** grows up to a full decagon, with an additional Zn_3 triangle and a partially occupied Sn outside the full decagon, forming the SBU **B** in $Ru_{4.15}Sn_{4.96}Zn_{5.85}$. SBUs **B** in $Ru_{4.15}Sn_{4.96}Zn_{5.85}$ are arranged in the same way as **A** in $Ru_2Sn_2Zn_3$. The close relationship between SBUs **A** and **B** results in the similar magnitude of the *a* and *b* lattice parameters of the two phases, whereas the *c* axes are considerably different, $a = 8.2219(16)$, $b = 4.1925(8)$, $c = 13.625(3)$ Å for $Ru_2Sn_2Zn_3$ and $a = 8.3394(17)$, $b = 4.2914(9)$, $c = 28.864(6)$ Å for $Ru_{4.15}Sn_{4.96}Zn_{5.85}$.

Symmetry incompatibility is a prominent feature of the SBU **B** in $Ru_{4.15}Sn_{4.96}Zn_{5.85}$. The internal angles of the real Ru_5Sn_5 decagon in **B** deviate from that of a perfect decagon (144°) by −4.66, +6.37, −5.21, +3.82, −0.79, +0.20, +3.48, −6.71, +4.66, and −1.19°, respectively, with an average of 3.70°. The averaged length of the edges of the real Ru_5Sn_5 decagon is 2.680(37) Å. The Ru and Sn atoms in the Ru_5Sn_5 decagon appear alternatively to form Ru_5 and Sn_5 pentagons. In the central triangle, one vertex splits into two sites Zn61 and Ru62 (with site occupancy factor $f_{Zn61} = 0.84$ and $f_{Ru62} = 0.16$), namely, $Zn_{2.84}Ru_{0.16}$. The internal angles are 61.53° (61.39°), 57.92° (65.28°), and 60.55° (53.33°) for the triangle containing Zn61 (Ru62). The distortions of these polygons can be scaled quantitatively using the *CShM* and *CSM*.[5] A value between 0 and 100 will be obtained by this method. The value is zero if the polygon exactly has the perfect shape and is proportional to the degree of distortion. The values of $S(C_5) = Sh$(perfect decagon) = 0.0487 given by the *CShM* and *CSM* indicate that the Ru_5Sn_5 polygon has a nearly perfect decagonal shape. The central $Zn_{2.84}$ triangle without Ru62 shows the symmetry features of $S(C_3) = Sh$(perfect triangle) = 0.0349. All the values indicate that the deviations of these polygons from their corresponding perfect regular shapes are very small.

It is important to emphasize the differences between the symmetrically incompatible unit $Zn_{2.84}Ru_{0.16}@Ru_5Sn_5$ (symbol @ means two polygons have the common center) in $Ru_{4.15}Sn_{4.96}Zn_{5.85}$ and other units with similar geometry in the literature. In the quasicrystal approximant ε_{16} in the Rh−Al system,[11] there also existed the decagonal units with triangle centers located in flat layers, such as

(11) Li, M. R.; Sun, J. L.; Oleynikov, P.; Hovmöller, S.; Zou, X. D.; Grushko, B. *Acta Crystallogr., Sect. B* **2010**, *66*, 17–26.

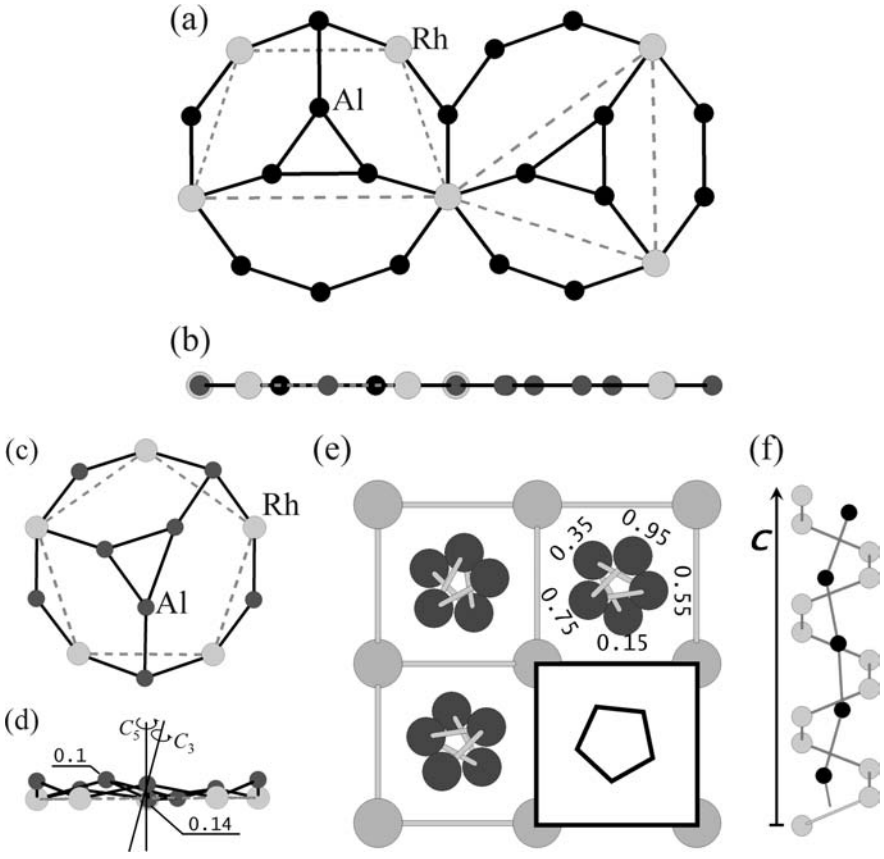

Figure 3. Coupling of two incompatible symmetries in (a−d) the Rh−Al decagonal quasicrystal approximant ε_{16} and (e−f) the Nowotny chimney ladder phase Ir_3Ga_5. The 3-fold axis C_3 of the central triangle and the 5-fold axis C_5 of the pentagon indicated by dashed lines in (c) are shown in (d). The numerals in (d) and (e) show the heights of the atoms along the *y* or *z* directions, respectively.

$Al_3@Rh_3Al_7$ and $Al_3@Rh_4Al_6$ as shown in Figure 3a,b. Taking the atomic types into account, however, the decagons Rh_3Al_7 and Rh_4Al_6 lost their 5-fold symmetry significantly because of the formation of the Rh_3 triangle and Rh_4 trapezoid as indicated by the dashed lines in Figure 3a. The $Al_3@Rh_5Al_5$ (Figure 3c) unit containing two pentagons Rh_5 and Al_5 is similar to the $Zn_{2.84}Ru_{0.16}$-$@Ru_5Sn_5$ unit, but the layer where the unit was located was highly puckered (Figure 3d). As we can see in Figure 3d, the puckering was caused by the displacement of Al atoms. All five Rh atoms still stay in the flat layer and retain the shape of the perfect pentagon. However, due to the puckering, the pentagon Al_5 lost its 5-fold symmetry, and the central triangle Al_3 was tilted such that its 3-fold axis C_3 deviated from the 5-fold axis C_5 of the pentagon Rh_5. The role of the puckering also can be explained by another example, namely, so-called Nowotny chimney ladder phases.[12] For example, if the unit cell of the Nowotny chimney ladder phase Ir_3Ga_5 is compressed into a layer perpendicular to the *c* axis, symmetry incompatibility between atoms in chimneys (Ir) and ladders (Ga) emerges, namely, between the square and pentagon in Figure 3e. In the real structure, however, chimneys and ladders extend along the *c* axis to form the structure with a Ga helix within an Ir helix, and the two helices had different period lengths (Figure 3f). The extension along the *c* axis can be considered as an extreme case of puckering. In our case, $Zn_{2.84}Ru_{0.16}@Ru_5Sn_5$ (nearly $C_3@C_5$) is located in an absolutely flat plane, and both the decagon and the triangle slightly deviate from the perfect polygons, as indicated by the very small values given by the *CSM* and *SChM* mentioned above.

In MCd_6 (M = Ca, rare-earth) approximants,[1] because the innermost tetrahedral cluster has lower symmetry than that of the outer icosahedral shells, which are symmetrically incompatible, it gains the degree of freedom in the orientation and is completely disordered. In many results,[13−15] the phase transition of the order−disorder type with respect to the orientations of the tetrahedrons in these crystalline approximants was observed. For different systems, the phase transition temperatures varied from ~80 K in $ScZn_6$[13] to ~500 K for $EuCd_6$.[14] It was also reported that the tetrahedron in $YbCd_6$ approximant exhibited five various types of orientational order sensitive to pressure and temperature.[15] These examples indicated that, in MCd_6 approximants, the orientations of the tetrahedrons is not only related to symmetry but also energy. Compared to the symmetrically incompatible polyhedrons in MCd_6, the decagon with a central triangle

(12) (a) Schwomma, O.; Nowotny, H.; Wittmann, A. *Monatsh. Chem.* **1964**, *95*, 1538–1543. (b) Jeitschko, W.; Parthé, E. *Acta Crystallogr.* **1967**, *22*, 417–430. (b) Fredrickson, D. C.; Lee, S.; Hoffmann, R.; Lin, J. H. *Inorg. Chem.* **2004**, *43*, 6151–6158.

(13) Tamura, R.; Nishimoto, K.; Takeuchi, S.; Edagawa, K.; Isobe, M.; Udea, Y. *Phys. Rev. B* **2005**, *71*, 092203.

(14) Nishimoto, K.; Tamura, R.; Takeuchi, S. *Phys. Rev. B* **2010**, *81*, 184201.

(15) Watanuki, T.; Machida, A.; Ikeda, T.; Aoki, K.; Kaneko, H.; Shobu, T.; Sato, T. J.; Tsai, A. P. *Phys. Rev. Lett.* **2006**, *96*, 105702.

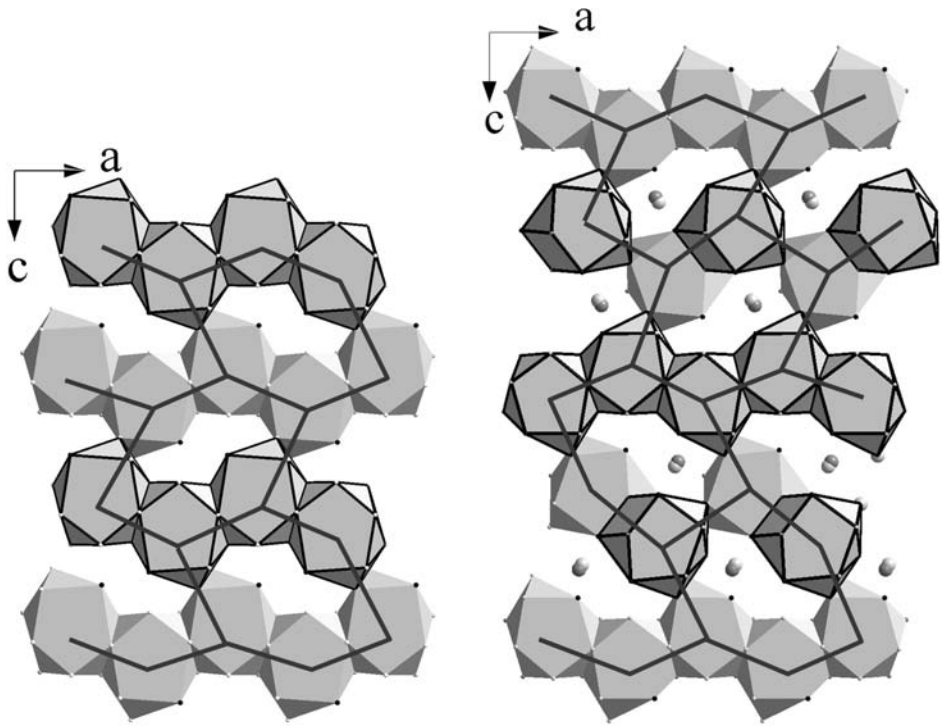

Figure 4. Structures of $Ru_2Sn_2Zn_3$ (left) and $Ru_{4.15}Sn_{4.96}Zn_{5.85}$ (right) shown in arrays of Sn-centered pentagonal antiprisms along the [010] direction, where the pentagonal antiprisms with higher and lower *b*-axis heights are represented by thick and thin edges, respectively. Connecting the centers of these antiprisms leads to periodic arrays of distorted hexagons highlighted by bold lines.

in $Ru_{4.15}Sn_{4.96}Zn_{5.85}$ is the case of two-dimensional symmetry incompatibility. As like the tetrahedron in MCd_6, significant disorder is expected for the central triangles, but it is very close to 3-fold symmetry except for a slight composition deviation at one vertex. The orientation and the degree of order of the central triangles might be explained by the following two facts:

(1) The chemical bonding within and between the layers where the decagons with central triangles are located is of the same character. The next layers have to be taken into account when the triangles try to find their "right" orientations. Viewed along the *b* axis, the triangle is sandwiched by two pentagons from the next layers. A closer check on the bond lengths implies that any remarkable rotation of the triangle around its 3-fold axis will result in an unreasonably short Zn−Sn bond.

(2) A systematic search indicated that the pseudosymmetry in the structures crystallized in the space group of *Pnma* implies a possible structural phase transition at elevated temperature.[16] In addition, the plot of the electrical resistivity as a function of temperature also showed a change in slope around 480 K (Figure 6). These two facts indicate a possible phase transition in $Ru_{4.15}Sn_{4.96}Zn_{5.85}$. As mentioned above, phase transitions of the order−disorder type were observed in MCd_6 approximants. Therefore, the relatively ordered structure of $Ru_{4.15}Sn_{4.96}Zn_{5.85}$ at room temperature may transform into a high-temperature phase with much more disorder. The high-temperature phase might be the structure with the space group of *Imma* as discussed in the part of structural determination. The disorders come from the mixed occupation between Sn and Ru in the decagon (0.5Sn and 0.5Ru on each site) and Zn and Ru at two vertices (not one in the room-temperature phase) of the central triangle (about 0.6Zn and 0.4Ru on each site). However, the XRD analysis showed that the phase decomposed into $Ru_2Sn_2Zn_3$ and Sn after it was annealed at 900 K for 10 h and then quenched in water.

In both structures of $Ru_2Sn_2Zn_3$ and $Ru_{4.15}Sn_{4.96}Zn_{5.85}$, these atomic layers stack along the *b* axis in the way that the neighboring layers are related to each other by a 2_1 screw axis. Projected along the *b* axis, both structures can be described by the arrays of Sn-centered pentagonal antiprisms (Figure 4). The differences between these two structures can be summarized as follows: (1) Connecting the centers of these pentagonal antiprisms leads to the arrays of distorted hexagons in both structures. The periodicity of the orientation of the hexagons in $Ru_{4.15}Sn_{4.96}Zn_{5.85}$ (.../ / \ \ / / \ \...) is twice longer than that in $Ru_2Sn_2Zn_3$ (.../ \ / \ ...). (2) The space surrounded by the pentagonal antiprisms is filled with the splitting Zn atoms in $Ru_{4.15}Sn_{4.96}Zn_{5.85}$ but not in $Ru_2Sn_2Zn_3$. (3) The rows of pentagonal antiprisms with different *b*-axis heights are present alternately in $Ru_2Sn_2Zn_3$, but there exist the rows composed of mixed *b*-axis heights in $Ru_{4.15}Sn_{4.96}Zn_{5.85}$.

Pentagonal columns have been of increasing interest because they might be ideal building units for two-dimensional quasi-crystalline structures. The most common pentagonal column is the interpenetrating icosahedral

(16) Igartua, J. M.; Aroyo, M. I.; Kroumova, E.; Perez-Mato, J. M. *Acta Crystallogr., Sect. B* **1999**, *55*, 177–185.

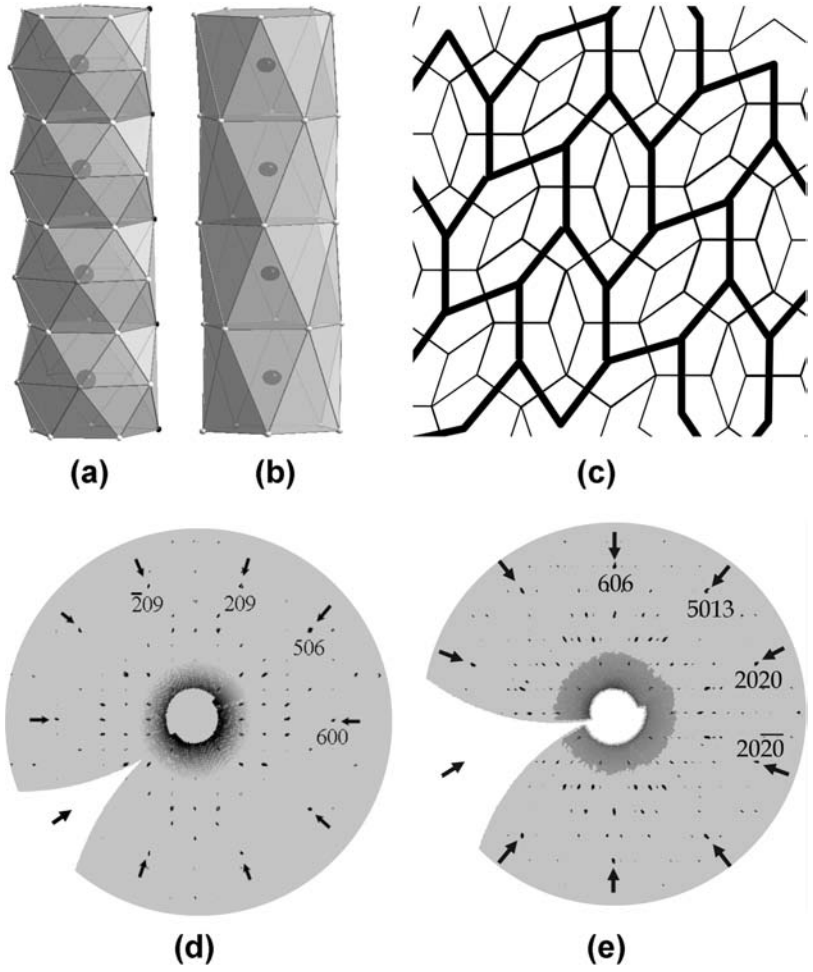

Figure 5. (a) Representative distorted Sn-centered pentagonal antiprism in the structures of $Ru_2Sn_2Zn_3$ and $Ru_{4.15}Sn_{4.96}Zn_{5.85}$; (b) typical pentagonal antiprism or interpenetrating icosahedral chain in previously reported structures; (c) periodic arrangement of pentagonal prisms in the structure of Al_3Mn decagonal quasicrystal approximants.[21] Reconstructed X-ray diffraction patterns of (d) $Ru_2Sn_2Zn_3$ and (e) $Ru_{4.15}Sn_{4.96}Zn_{5.85}$ show the pseudodecagonal intensity distribution highlighted by arrows in the *h*0*l* section.

chain as shown in Figure 5b, in which the coordination number of the centered atoms is 12.[6,17,18] In this work, an unexpected pentagonal antiprism is observed. Unlike the center atom sandwiched by two pentagons in Figure 5b, the centered Sn atom in Figure 5a is located in the middle of an expanded pentagon. The expanded pentagon is sandwiched by two smaller pentagons without centered atoms, resulting in that the atomic coordination number of the center atom is fifteen. A similar hexagonal antiprism present in the Ca coordination was reported in $CaCu_5$ type structures.[19] One can obtain the pentagonal antiprisms in the title compounds by replacing the staggered hexagons in the hexagonal antiprism with staggered pentagons. To the best of our knowledge, this new antiprism with staggered pentagons is reported for the first time.

The Penrose tiling pattern succeeded in describing the structures of both three-dimensional icosahedral quasicrystals and two-dimensional decagonal quasicrystals. In the original Penrose tiling, one uses pentagons and three other shapes: a five-pointed "star" (a pentagram), a "boat" (roughly 3/5 of a star), and a "diamond" (a thin rhombus).[20] If the centers of the pentagons are connected, we obtain a pattern composed of hexagons (H), boats (B), and stars (S), namely, HBS tiling.[20] Ideal quasiperiodic as well as periodic HBS structures are often used to describe decagonal quasicrystal phases and related crystalline approximants.[21,22] As shown in Figure 4, slightly distorted hexagonal arrays of pentagonal antiprisms are observed in both structures. These patterns remind us of the patterns reported in the approximants $Al_{13}Co_4$[23] and Al_3Mn,[21] in which the crystal structures are composed of alternately oriented prolate hexagonal subunits (H), as shown in Figure 5c. Accordingly, reconstructed X-ray diffraction patterns of both $Ru_2Sn_2Zn_3$ and $Ru_{4.15}Sn_{4.96}Zn_{5.85}$ (Figure 5d,e) show pseudodecagonal intensity distributions

(17) Kaskel, S.; Corbett, J. D. *Inorg. Chem.* **2000**, *39*, 3086–3091.
(18) (a) Li, X. Z.; Dubois, J. M. *J. Phys.: Condens. Matter* **1994**, *6*, 1653–1662. (b) He, Z. B.; Kuo, K. H. *J. Alloys Compd.* **2004**, *373*, 39–47. (c) Kuo, K. H.; Deng, D. W. *J. Alloys Compd.* **2004**, *376*, L5–L9.
(19) Bruzzone, G. *J. Less-Common Met.* **1971**, *25*, 361–366.
(20) Steurer, W.; Deloudi, S. In *Crystallography of Quasicrystals: Concepts, Methods and Structures*; Springer Series in Materials Science 126; Hull, R., Parisi, J., Osgood, R. M., Warlimont, H., Eds.; Springer: 2009; pp 21−31.
(21) (a) Li, X. Z.; Shi, D.; Kuo, K. H. *Philos. Mag. B* **1992**, *66*, 331–340. (b) Li, X. Z. *Acta Crystallogr., Sect. B* **1995**, *51*, 265–270. (c) Gummelt, P.; Bandt, C. *Mater. Sci. Eng., A* **2000**, *294*, 250–253.
(22) (a) Sui, H. X.; Sun, K.; Kuo, K. H. *Philos. Mag. A* **1997**, *75*, 379–393. (b) Wu, J. S.; Li, X. Z.; Kuo, K. H. *Philos. Mag. Lett.* **1998**, *77*, 359–370. (c) Wu, J. S.; Ge, S. P.; Kuo, K. H. *Philos. Mag.* **1999**, *A79*, 1787–1803.
(23) Fleischer, F.; Weber, T.; Jung, D. Y.; Steurer, W. *J. Alloys Compd.* **2010**, *500*, 153–160.

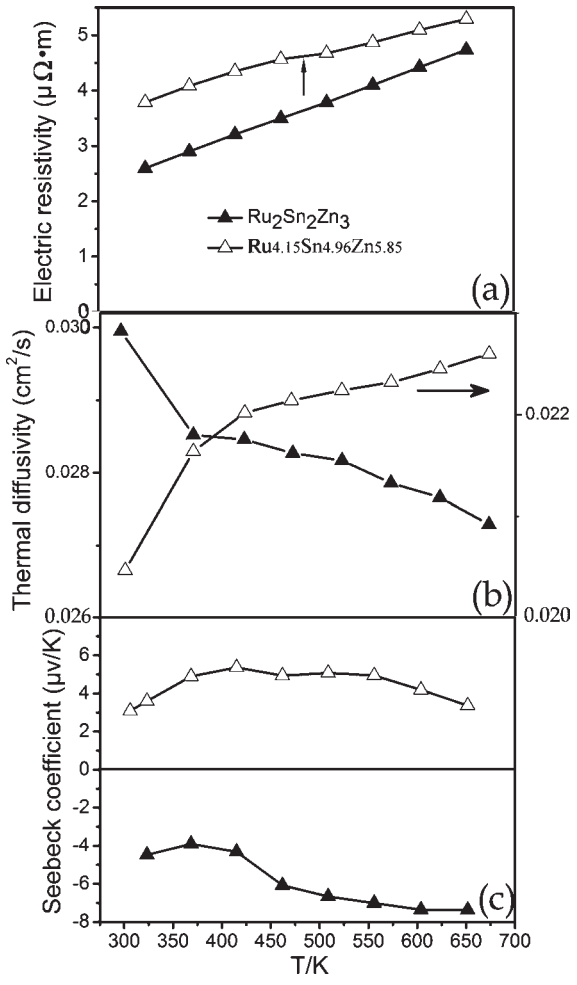

Figure 6. Temperature dependence of electrical resistivity (a), thermal diffusivity (b), and Seebeck coefficient (c) for $Ru_2Sn_2Zn_3$ and $Ru_{4.15}Sn_{4.96}Zn_{5.85}$. The arrow in (a) indicates the change in slope around 480 K.

in the *h*0*l* section. Since no quasicrystal phases have been reported in the Ru−Sn−Zn ternary system up to now, we classify the compounds $Ru_2Sn_2Zn_3$ and $Ru_{4.15}Sn_{4.96}Zn_{5.85}$ as a new family of pseudodecagonal approximants because of (a) their pseudodecagonal diffractions in the *h*0*l* section and (b) their point group *mmm* (subgroup of 10/*mmm* which is the diffraction pattern symmetry of decagonal quasicrystal).[24] This feature hints at the possibility that chemical modification may enable us to obtain quasicrystals in chemically varied systems.

Physical Properties. The temperature dependence of electrical resistivity for $Ru_2Sn_2Zn_3$ and $Ru_{4.15}Sn_{4.96}Zn_{5.85}$ indicates that both compounds are metallic as shown in Figure 6a. The values of electrical resistivity of $Ru_{4.15}Sn_{4.96}Zn_{5.85}$ are slightly larger than those for $Ru_2Sn_2Zn_3$. There is a change in slope around 480 K in the electrical resistivity for $Ru_{4.15}Sn_{4.96}Zn_{5.85}$, while that of $Ru_2Sn_2Zn_3$ increases linearly with the increasing temperature. The Seebeck coefficient for $Ru_2Sn_2Zn_3$ is negative while that for $Ru_{4.15}Sn_{4.96}Zn_{5.85}$ is positive. One of the possibilities leading to the positive Seebeck coefficient for $Ru_{4.15}Sn_{4.96}Zn_{5.85}$ is the deficiencies in the Sn5 site because the dangling bonds surrounding the Sn vacancies accept the carrier electrons so that the hole contribution becomes dominant. The larger electrical resistivity for $Ru_{4.15}Sn_{4.96}Zn_{5.85}$ may be attributed also to the reduced number of electrons due to the introduction of the vacancies. Their thermal diffusivities show opposite tendency with the increasing of temperature, and the positive temperature coefficient in $Ru_{4.15}Sn_{4.96}Zn_{5.85}$ possibly indicates bipolar contribution at higher temperature. The specific heat capacities at room temperature are 0.395 and 0.325 J/(g K) for $Ru_2Sn_2Zn_3$ and $Ru_{4.15}Sn_{4.96}Zn_{5.85}$, respectively. The thermal conductivity at room temperature was calculated from $\kappa = \rho\alpha C_p$, where ρ is the density of material, α is the thermal diffusivity, and C_p is the specific heat capacity, leading to 7.7 and 4.4 W/mK at room temperature for $Ru_2Sn_2Zn_3$ and $Ru_{4.15}Sn_{4.96}Zn_{5.85}$, respectively.

Conclusions

In summary, we identified two new ternary pseudodecagonal approximants $Ru_2Sn_2Zn_3$ and $Ru_{4.15}Sn_{4.96}Zn_{5.85}$. Both structures can be described by the hexagonal arrays of Sn-centered novel pentagonal antiprisms. With the increase in the Sn content, the half-decagonal structure unit with a triangle center in $Ru_2Sn_2Zn_3$ grows up to a symmetry incompatible decagonal unit with a central triangle in the common plane in $Ru_{4.15}Sn_{4.96}Zn_{5.85}$. They are remarkable examples to study the symmetry incompatibility in a two-dimensional plane and could be served as a simplified model for understanding the formation of decagonal quasicrystals and related compounds.

Acknowledgment. D.B.X. thanks the Alexander von Humboldt Foundation (Germany) and Japan Society for the Promotion of Science for postdoctoral fellowships. Fruitful discussion with Prof. Bernd Harbrecht and his great supports on experiments in Germany are gratefully acknowledged. Acknowledgements are made to Prof. David Avnir, Prof. Pere Alemany, and Dr. Chaim Dryzun for their willingness to share their computer programs for analysis of continuous shape and symmetry measures and fruitful discussion.

Supporting Information Available: Figure S1−S4 (powder X-ray diffraction patterns and analyses and EDS) and CIF data. This material is available free of charge via the Internet at http://pubs.acs.org.

(24) Boström, M.; Hovmöller, S. *J. Solid State Chem.* **2000**, *153*, 398–403.